BBA - Bioenergetics 1864 (2023) 148983

Contents lists available at ScienceDirect

BBA - Bioenergetics

journal homepage: www.elsevier.com/locate/bbabio

Exploring substrate interaction in respiratory alternative complex III from *Rhodothermus marinus*

Filipa Calisto [a], Smilja Todorovic [b], Ricardo O. Louro [b], Manuela M. Pereira [a,*]

[a] University of Lisbon, Faculty of Sciences, Department of Chemistry and Biochemistry and BioISI - Biosystems & Integrative Sciences Institute, Campo Grande, C8, 1749-016 Lisboa, Portugal

[b] Instituto de Tecnologia Química e Biológica – António Xavier, Universidade Nova de Lisboa, Av. da República EAN, 2780-157 Oeiras, Portugal

ARTICLE INFO

Keywords:
Alternative complex III (ACIII)
Cytochrome *bc*1
Menaquinone
High Potential Iron Sulfur Protein (HiPIP)
Thermophile
Respiratory chain

ABSTRACT

Rhodothermus marinus is a thermohalophilic organism that has optimized its microaerobic metabolism at 65 °C. We have been exploring its respiratory chain and observed the existence of a quinone:cytochrome *c* oxidoreductase complex, named Alternative Complex III, structurally different from the bc_1 complex. In the present work, we took profit from nanodiscs and liposomes technology to investigate ACIII activity in membrane-mimicking systems. In addition, we studied the interaction of ACIII with menaquinone, its potential electron acceptors (HiPIP and cytochrome *c*) and the caa_3 oxygen reductase.

1. Introduction

Rhodothermus marinus is a thermohalophilic bacterium, isolated from shallow-water submarine alkaline hot springs in Iceland and the Azores [1,2]. It is a strict aerobic Gram-negative bacterium with an optimum growth temperature of 65 °C and a sodium concentration of 1–2 % [1,2]. We have been carrying out an exhaustive characterization of the respiratory chain from *R. marinus* [3–10] (Fig. 1) and identified for the first time a quinol:electron acceptor oxidoreductase named Alternative Complex III (ACIII), because it is functionally but not structurally equivalent to cytochrome bc_1 complex of bacteria and complex III of the mitochondrial respiratory chain [3,10–14].

ACIII is a membrane complex that transfers electrons from quinol to periplasmatic proteins, such as a High Potential Iron-sulfur Protein (HiPIP) or a soluble cytochrome *c* [4,9–11]. Both the HiPIP and the soluble cytochrome *c* were previously observed to be electron donors to the caa_3 oxygen reductase [3,4,9]. ACIII from *R. marinus* is composed of eight subunits, encoded by the gene cluster *actABCDEFG*, six of which are conserved across species (*actA* to *actF*) and the isolated gene *actH* [15]. ActA, ActB and ActE are periplasmic subunits and accommodate all the prosthetic groups in the complex. ActA harbors five *c*-type hemes [10]. ActE is a monoheme cytochrome *c* and was previously proposed to be the last electron acceptor within ACIII [9,15]. ActB is composed of two different domains, designated as B1 and B2, homologous to the catalytic and the iron-sulfur subunits of the members of the complex iron-sulfur molybdoenzyme (CISM) family, respectively [13]. ActB has three $[4Fe\text{-}4S]^{2+/1+}$ and one $[3Fe\text{-}4S]^{1+/0}$ and no molybdopterin (in contrast to the members of the CISM family). The prosthetic groups of ACIII (the *c*-type hemes and the iron-sulfur clusters) form a branched electron transfer wire that diverge at the $[3Fe\text{-}4S]^{1+/0}$ cluster [10]. ActC and ActF are membrane proteins homologous to each other and members of the NrfD-family [10,16,17]. One quinol-binding site was identified in ActC, close to the $[3Fe\text{-}4S]^{1+/0}$ cluster of ActB [10]. The existence of putative proton pathways was observed in ActC and ActF, and proposed to all NrfD-subunits [10,16]. ActD is a transmembrane subunit suggested to play a significant role in ACIII coupling mechanism. ActG is predicted to be a transmembrane subunit and ActH is a peripheral protein most probably with a structural role [10,18]. The structure of ACIII suggests that ACIII is a redox-driven proton pump [10,19].

Genes coding for ACIII are spread among Bacteria and, in some species, they co-exist with genes encoding cytochrome bc_1 complex [15,20]. The gene cluster coding for ACIII is frequently followed by a gene cluster coding for an oxygen reductase, as in the case of *R. marinus*. In fact, in the membranes of *R. marinus*, ACIII and caa_3 oxygen reductase were shown to be structurally and functionally associated [9,15]. The caa_3 oxygen reductase [4], is a typical member of type A2 subfamily of heme-copper oxygen reductases [3,21], being composed of four subunits, with a total of five redox centers. It reduces oxygen to water in a reaction coupled to proton pumping [4]. The cytochrome *c* domain of

* Corresponding author.
E-mail address: mmpereira@fc.ul.pt (M.M. Pereira).

https://doi.org/10.1016/j.bbabio.2023.148983
Received 19 January 2023; Received in revised form 4 April 2023; Accepted 20 April 2023
Available online 29 April 2023

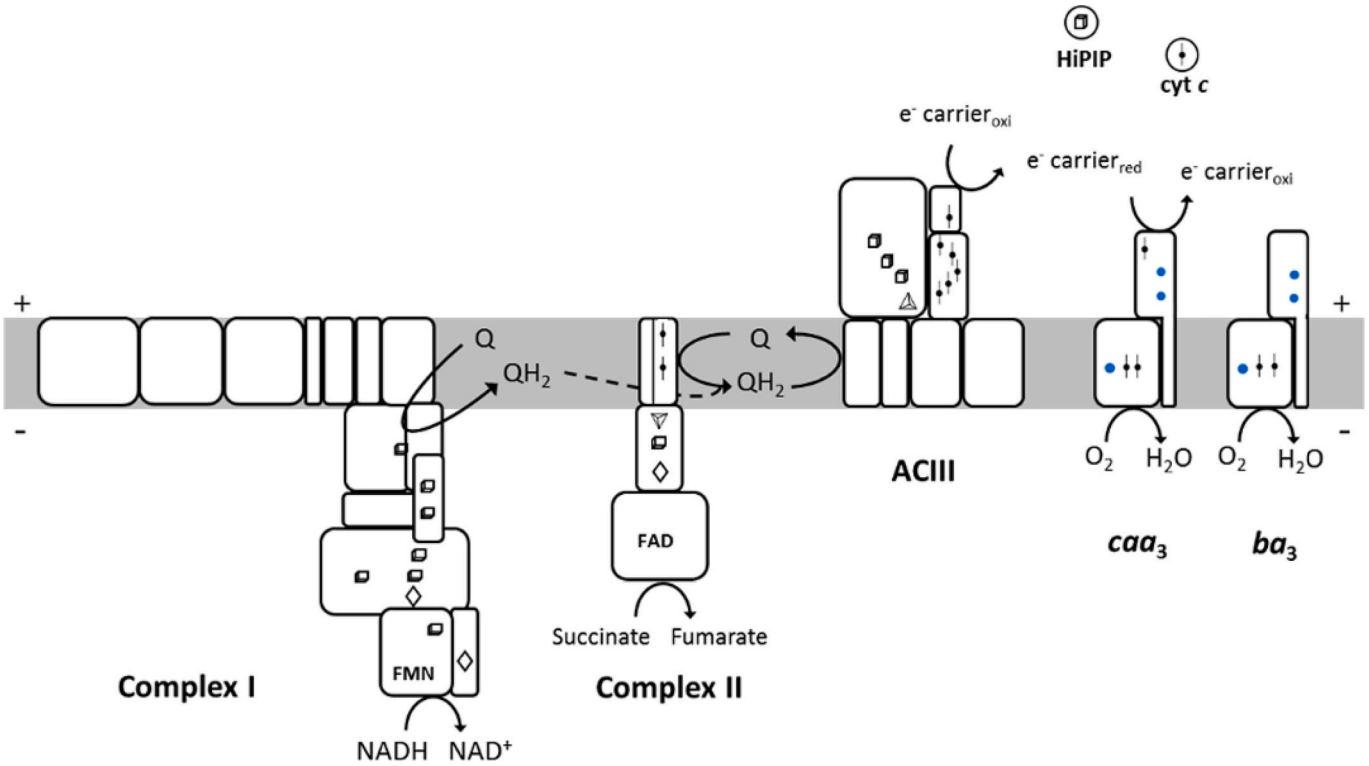

Fig. 1. Schematic representation of *Rhodothermus marinus* respiratory chain. The respiratory chain of *R. marinus* is composed of NADH:quinone oxidoreductase (complex I) [6], succinate:quinone oxidoreductase (complex II) [5], the alternative complex III (ACIII) [12], the caa_3 oxygen reductase, a type A2 enzyme of the Heme-copper oxidase superfamily [4] and, the ba_3 oxygen reductase, a type B enzyme of the Heme-copper oxidase superfamily [7]. FMN represents the Flavin mononucleotide. Cubes, pyramids, and diamonds represent [4Fe-4S], [3Fe-4S] and [2Fe-2S] clusters, respectively. *c*-type hemes are represented as ball and stick, and the copper metal centers as blue spheres. (For interpretation of the references to colour in this figure legend, the reader is referred to the web version of this article.)

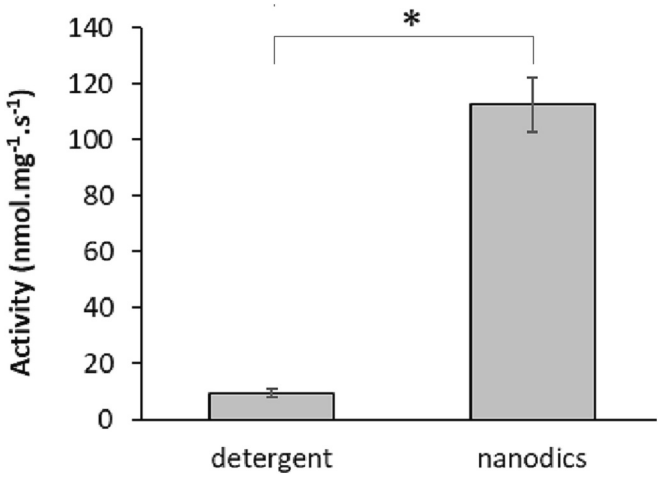

Fig. 2. Catalytic activity of ACIII. Menaquinol:cytochrome *c* oxidoreductase activity of ACIII solubilized in detergent or reconstituted in nanodiscs. * $p < 0.05$ as determined by Student's-*t*-test.

subunit II was indicated to be the electron entering point in the caa_3 reductase [22].

The study here presented explored the interaction of ACIII from *R. marinus* with the different substrates; menaquinone, HiPIP, and cytochrome *c*, and with the caa_3 oxygen reductase. We took profit from nanodiscs and liposomes technology to investigate ACIII activity in a membrane mimicking system.

2. Materials and methods

2.1. Bacterial growth and protein purification

Rhodothermus marinus strain PRQ-62B growth was carried out as described previously and ACIII was purified according to optimized procedures [3,12].

The heterologous production and purification of the soluble truncated version of monoheme cytochrome *c* subunit of ACIII (ActE), as well as of the soluble periplasmatic proteins of *R. marinus*, the monoheme cytochrome *c* (cytC) and the High Potential Iron-sulfur Protein (HiPIP), and the cytochrome *c* domain of caa_3 oxygen reductase (domC) were performed as described before [9,22–24].

The reduction of 2 μM of ACIII with 10 μM of menaquinol-4 was measured spectrophotometrically inside an anaerobic chamber, using an UV–visible spectrophotometer, following heme reduction at 553 nm. Experiments were performed in 20 mM Tris-HCl pH 7.6, 150 mM NaCl and 0.03 % DDM, with constant stirring and the temperature was kept at 65 °C.

2.2. Reconstitution of ACIII into nanodiscs and liposomes

The reconstitution of ACIII and caa_3 oxygen reductase into nanodiscs was carried out following the guidelines described before [25]. Briefly, the expression of the membrane scaffold protein (MSP1E1) was achieved using *E. coli* BL21-GOLD (DE3) strain as host and the plasmid pMSP1D1 (Addgene #20062) [26]. LB medium containing 30 μg/mL kanamycin was inoculated with single colony from a fresh growth in solid medium and the culture was grown at 37 °C with shaking (250 rpm). Induction of gene expression with 1 mM IPTG was performed when OD_{600} reached 1. For the purification of MSP1E1, *E. coli* cells were harvested at four hours after induction by centrifugation and the pellet

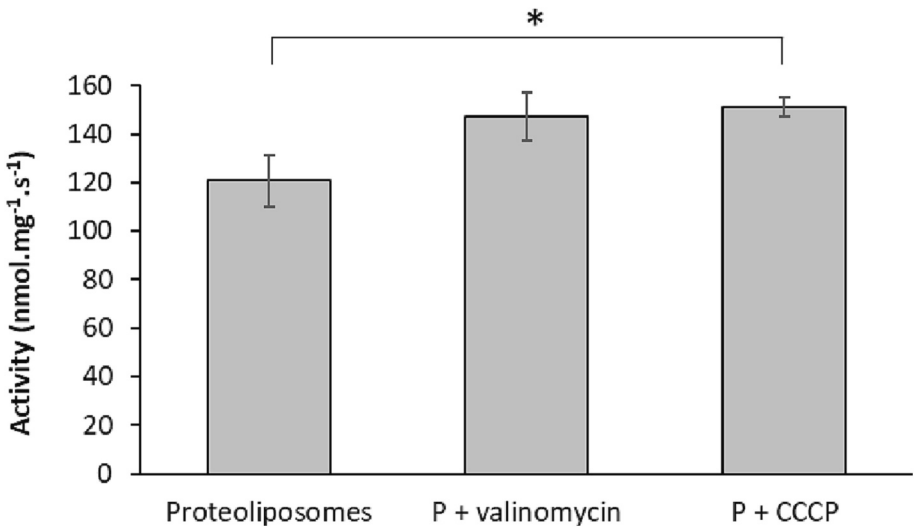

Fig. 3. Menaquinol:cytochrome *c* oxidoreductase activity of ACIII reconstituted in liposomes. Cytochrome *c* reduction by proteoliposomes containing ACIII (P) was analyzed in the absence or in the presence of valinomycin (P + valinomycin) or protonophore CCCP (P + CCCP). * $p < 0.05$ as determined by Student's *t*-test.

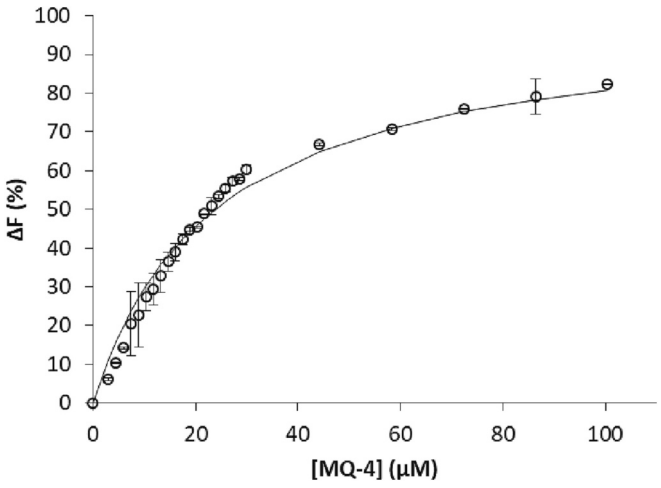

Fig. 4. Menaquinone interaction with ACIII. Change in the fluorescence emission at 340 nm with excitation at 295 nm of ACIII upon sequential addition of menaquinone-4 (MQ-4), open circles. Eq. (1) was used to obtain the dissociation constant (K_d).

resuspended in 20 mM Tris-HCl pH 7.5. The cells were then disrupted by passing through a French Press at 19,000 psi and the unbroken cells were removed by centrifugation at 22,000 *g* for 15 min at 4 °C. Soluble and membrane fractions were separated by centrifugation at 200,000 *g*, for 2 h at 4 °C. The soluble fraction, containing the MSP1E1, was loaded into a Histrap column (GE-Heathcare) and eluted in a linear gradient of 1 M imidazole from 0 to 100 %, in 20 mM Tris-HCl pH 7.5, 500 mM NaCl. 1–1-palmitoyl-2-oleoyl-glycero-3-phosphocholine (POPC) and cardiolipin lipids (CL), from Avanti Polar Lipids, were solubilized in chloroform and then extensively dried at low pressure at 37 °C to remove all traces of organic solvents. The washed lipids were resuspended in 20 mM Tris-HCl pH 7.5 containing 200 mM sodium cholate and 150 mM NaCl. Cholate solubilized lipids were mixed with MSP1E1, menaquinone-4 (5 mg/mL, Merck) and detergent solubilized ACIII in a proportion of, approximately, 128: 2:1 (lipids:MSP1E1:ACIII). After incubating the mixture at 25 °C for 2 h, detergent was eliminated by the addition of Bio-Beads SM-2 at 4 °C overnight. At the end, Bio-Beads were removed and nanodiscs assembly was analyzed by size exclusion chromatography. Reconstitution of ACIII into nanodiscs was also performed in the presence of 1 mM of the inhibitor 2-heptyl-4-hydroxyquinoline-N-oxide (HQNO, Enzo), when referred.

For the reconstitution of ACIII into liposomes, 20 mg of *E. coli* polar lipid extract (Avanti) were dissolved in chloroform and dried at low pressure at 37 °C until a lipid film was formed. The lipid film was dissolved in 500 μL of 10 mM HEPES-Tris pH 7.5, 50 mM Na_2SO_4, 50 mM K_2SO_4 and passed through a 0.2 μm membrane filter at least twenty-one times using a mini-extruder apparatus. The resulting liposome sample was twice frozen in liquid nitrogen and thawed in water. 100 μg of purified ACIII, 20 μL cholate (20 % stock solution) and 500 μL of liposome suspension were incubated for 30 min at room temperature. The sample was dialyzed overnight against the same buffer at 4 °C. Integrity of proteoliposomes was analyzed by generating K^+ gradients with 10 μM valinomycin in an external buffer containing 100 mM K_2SO_4, following oxonol VI absorption (Abs_{628} minus Abs_{587}) in an OLIS upgraded Aminco DW2 dual wavelength spectrophotometer, at 37 °C.

2.3. Activity assays

Menaquinol:electron acceptor oxidoreductase activity of ACIII was measured at 65 °C on a Shimadzu UV-1800 spectrophotometer inside an anaerobic chamber, using either ACIII solubilized in DDM, incorporated into nanodiscs or liposomes. Menaquinol-4, used as electron donor, was prepared according to Ragan et al. (1987) [27]. The reaction mixture contained ACIII in the nM range, 30 μM menaquinol-4 and 50 μM of electron acceptor. The reaction was started by the addition of ACIII and menaquinol-4, previously incubated, and monitored by following the reduction of the electron acceptors at 551 nm for domC, cytC or horse heart cytochrome *c* (eqCyt), an alternative to the physiological substrates, or at 480 nm for the HiPIP. The extinction coefficients used for domC, cytC, eqCyt and HiPIP were 21 mM^{-1} cm^{-1}, 21 mM^{-1} cm^{-1}, 18.5 mM^{-1} cm^{-1} [28] and 10 mM^{-1} cm^{-1}, respectively. All the assays were conducted in 50 mM potassium phosphate buffer at pH 7.5 at 65 °C in the presence of 0.2 mM EDTA, 1 mM NaN_3, 250 mM sucrose, 0.1 % BSA and 2 mM $Ca(OAc)_2$. When referred, experiments with liposomes were supplemented with 20 μM K^+ ionophore valinomycin (Merck) or 20 μM protonophore carbonyl cyanide ɱ-chlorophenyl hydrazone (CCCP, Merck). Turnover numbers are expressed as mol of electron acceptor reduced per mol of ACIII per second and the specific activity as nmol. $mg^{-1}.s^{-1}$.

The activity temperature profile was performed for ACIII nanodiscs at 200 mM potassium phosphate at pH 7.5 and between 40 and 80 °C. All the values were obtained from three independent assays.

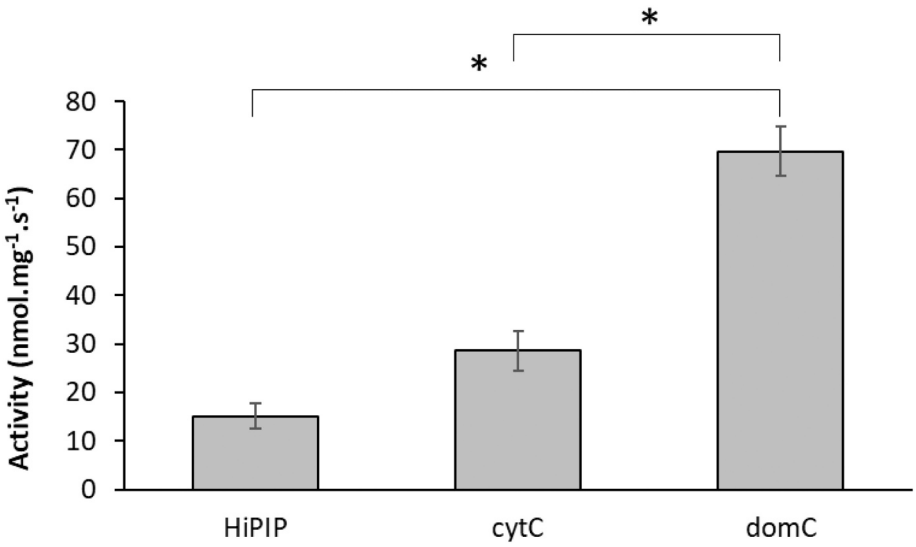

Fig. 5. Menaquinol:electron acceptor oxidoreductase activity of ACIII. The activity of ACIII reconstituted in nanodiscs was evaluated using the high potential iron-sulfur protein (HiPIP), the soluble cytochrome *c* (cytC) and the cytochrome *c* domain of the subunit II from the caa_3 reductase (domC) as electron acceptors. * $p < 0.05$ as determined by Student's *t*-test.

2.4. Tryptophan fluorescence titration

Fluorescence spectra of ACIII were obtained on a Varian Cary Eclipse spectrofluorometer. The reaction mixture (500 μL) contained 2 μM ACIII in 50 mM potassium phosphate pH 7.0 and 0.03 % DDM. The interaction of menaquinone-4 with ACIII was evaluated by monitoring the changes in the tryptophan fluorescence emission spectrum excited at 295 nm at 65 °C. Three independent titrations were performed in the range of 0 to 100 μM. The change in emission at 340 nm (ΔF) was normalized and plotted *vs* menaquinone-4 concentration. Dissociation constant (K_d) and maximum fluorescence (ΔF_{max}) values were computed based on the data fitted with the equation:

$$\Delta F = \frac{\Delta F_{max}.[S]}{K_d + [S]} \quad (1)$$

where ΔF represents the percent change in fluorescence intensity relative to the initial value after addition of quinone at a concentration $[S]$, and ΔF_{max} is the maximum percent quenching of the fluorescence intensity that occurs upon saturation of the substrate-binding site [29].

2.5. ^{1}H-1D-NMR titrations

Protein samples (HiPIP, ActE, domC and cytC), previously oxidized with potassium ferricyanide, were dialyzed against 20 mM potassium phosphate buffer pH 7.5, prepared in deuterium oxide (99.9 atom % D). Samples were concentrated using VivaSpin concentrators with cutoffs of 5 or 10 kDa. The final concentration of the samples, determined by UV–visible spectroscopy using the extinction coefficients referred above, was approximately 2 mM. 150 μM of ActE was titrated by increasing concentrations of HiPIP, domC or cytC. ^{1}H-1D-NMR spectra were recorded after each addition. The chemical shifts of the resonances corresponding to the methyl groups of the heme of ActE were measured in each spectrum. All ^{1}H-1D-NMR experiments were performed at 40 °C on a Bruker Avance II 500 MHz spectrometer operating at 500 MHz equipped with a TXI probe.

Chemical shifts of the resonances are presented in ppm and only values equal or larger than 0.012 were considered significant, smaller values are of insufficient magnitude for a confident estimation of binding parameters [30]. When several methyl resonances from the ActE heme were clearly visible, the data obtained for all methyl groups were used to define the dissociation constant. The NMR spectra were processed and analyzed with Bruker TopSpin program. Chemical shift changes ($\Delta\delta_{bind}$) of the NMR resonances from heme methyl groups of ActE were plotted against the molar ratio (R) of the titrants [30]. Data were fitted by least squares minimization using a 1:1 binding model with the following equations[31]:

$$\Delta\delta_{bind} = \frac{1}{2}\Delta\delta^{\infty}_{bind}\left(A - \sqrt{A^2 - 4R}\ \right) \quad (2)$$

$$A = 1 + R + \frac{K_d\left([P_A]_0\, R + [P_B]_0\ \right)}{[P_A]_0\ [P_B]_0} \quad (3)$$

where $\Delta\delta^{\infty}_{bind}$ is the maximal chemical shift perturbation of the NMR signals resulting from the complex formation between protein A (P_A) and protein B (P_B), K_d is the dissociation constant, $[P_A]_0$ is the initial concentration of protein A, and $[P_B]_0$ is the stock concentration of the titrant, protein B.

2.6. Resonance Raman (RR) studies

Approximately 0.2 mM of ACIII (in 20 mM Tris-HCl pH 7.5150 mM NaCl) as prepared, dithionite reduced or incubated with 2 mM of menaquinol-4, was introduced into a liquid nitrogen-cooled cryostat (Linkam THMS600) mounted on a microscope stage and cooled to −190 °C. RR spectra of the frozen sample were collected in backscattering geometry using a confocal microscope coupled to the Raman spectrometer (Jobin Yvon U1000), and the 413 nm excitation line from a krypton ion laser (Coherent Innova 302). Spectra were accumulated for 4 × 20 s with a laser power at sample of 10 mW. All spectra were subjected to polynomial baseline subtraction; the positions and widths of Raman bands were determined by component analysis as described previously [32].

3. Results

This work aimed at exploring the electron transfer from the quinone pool to oxygen, revealing the preferential electron transfer mode in *R. marinus* respiratory chain. Therefore, we performed kinetic assays monitored by UV–visible spectroscopy and protein-substrate interaction studies using fluorescence, NMR and Raman spectroscopies to investigate the redox activity of ACIII and the interaction between ACIII and its substrates.

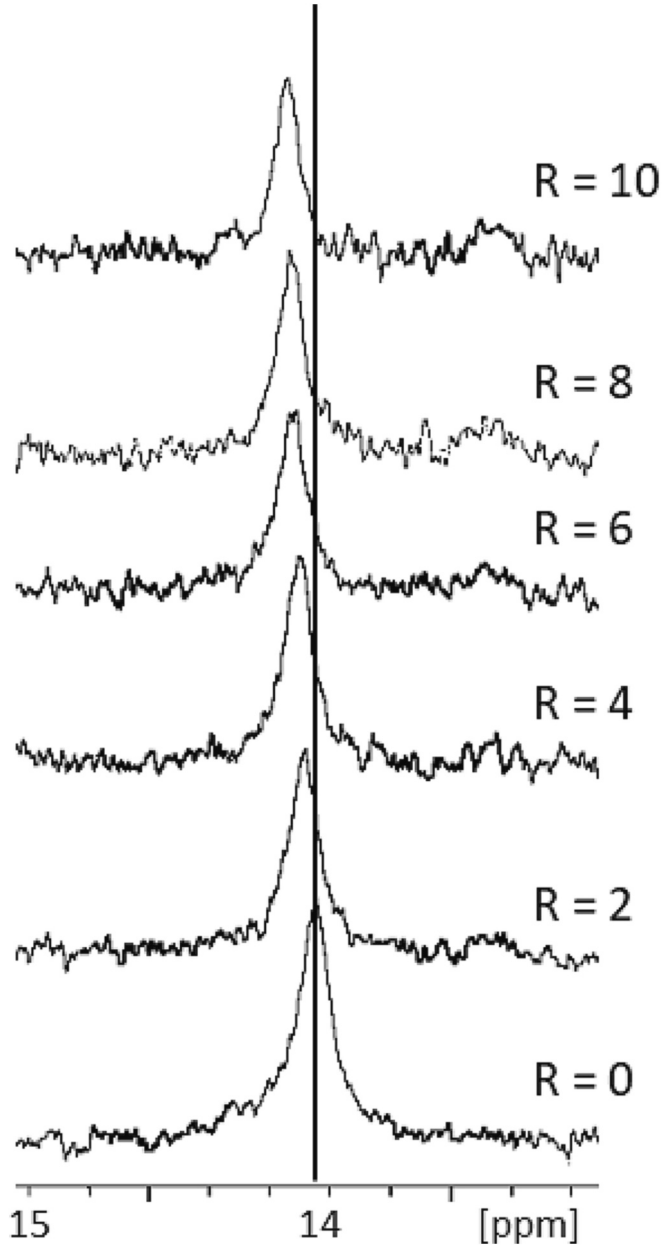

Fig. 6. ^{1}H-1D-NMR spectral changes of the signal from a methyl group of ActE. Changes of the signal from the methyl group at 14 ppm belonging to the heme of the monoheme cytochrome *c* subunit (ActE) of ACIII in the presence of increasing amounts of HiPIP, illustrating the data used in the chemical shift perturbation analysis. The *R* values correspond to the molar ratio of HiPIP and ActE.

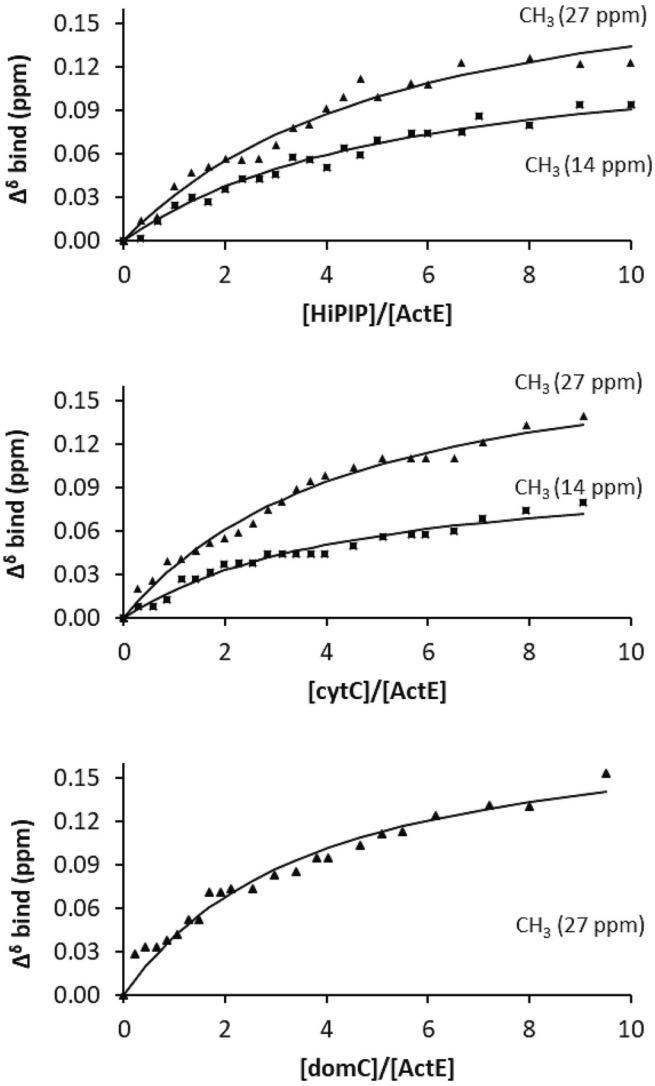

Fig. 7. Interaction of ActE from ACIII with different electron acceptors. Binding curves for the heme methyl groups of ActE that showed interactions, monitored by ^{1}H-1D-NMR spectroscopy. The chemical shift perturbations of the heme methyl signals are plotted as a function of the molar ratio of the interacting proteins. The solid lines represent the fit of Eq. 3 to chemical shift perturbations for the selected methyl groups.

3.1. Activity of ACIII

Menaquinol:cytochrome *c* oxidoreductase activity of detergent solubilized ACIII was measured by monitoring spectroscopically the reduction of horse heart cytochrome *c* (eqCyt) using menaquinol-4 as the electron donor. The ACIII turnover, in detergent solution, was 2.5 ± 0.4 s^{-1} (9.5 ± 1.4 nmol.mg^{-1}.s^{-1}) (Fig. 2, detergent). Since this menaquinol:cytochrome *c* oxidoreductase activity value was lower than the activity described for the ACIII from *Chloroflexus aurantiacus*, 45.6 ± 0.8 s^{-1} [33], we hypothesized that some important components, such as phospholipids or intrinsically bound quinones, which could affect the activity of the complex, might have been lost during the purification procedure. We tested this hypothesis reconstituting the detergent solubilized ACIII in membrane-mimicking environments. ACIII was first reconstituted in nanodiscs containing 1-1-palmitoyl-2-oleoyl-glycero-3-phosphocholine (POPC), 18:0 cardiolipin and menaquinone-4 in a proportion of approximately 128:2:1 (lipids:MSP1E1:ACIII). The activity of ACIII reconstituted into nanodiscs was significantly higher than that measured in detergent solubilized conditions, 19.9 ± 2.1 s^{-1} (74.7 ± 4.5 nmol.mg^{-1}.s^{-1}). This clearly shows the influence of phospholipids in the catalytic activity of the complex, possibly in the stabilization of ACIII. To examine whether cardiolipin stimulates ACIII activity, we prepared nanodiscs only with POPC. In the absence of cardiolipin the menaquinol:cytochrome *c* oxidoreductase activity of ACIII could not be restored, which demonstrates that cardiolipin is important for ACIII activity (data not shown).

As menaquinone-4 is hardly soluble in aqueous solution, we reconstituted ACIII into nanodiscs containing POPC and cardiolipin in the presence of menaquinone-4 and the activity of ACIII increased to 29.9 ± 2.6 s^{-1} (112.5 ± 10 nmol.mg^{-1}.s^{-1}) (Fig. 2, nanodiscs), probably due to the stabilization of menaquinone-4. On the other hand, reconstitution of ACIII into nanodiscs in the presence of menaquinone-4 and HQNO, a

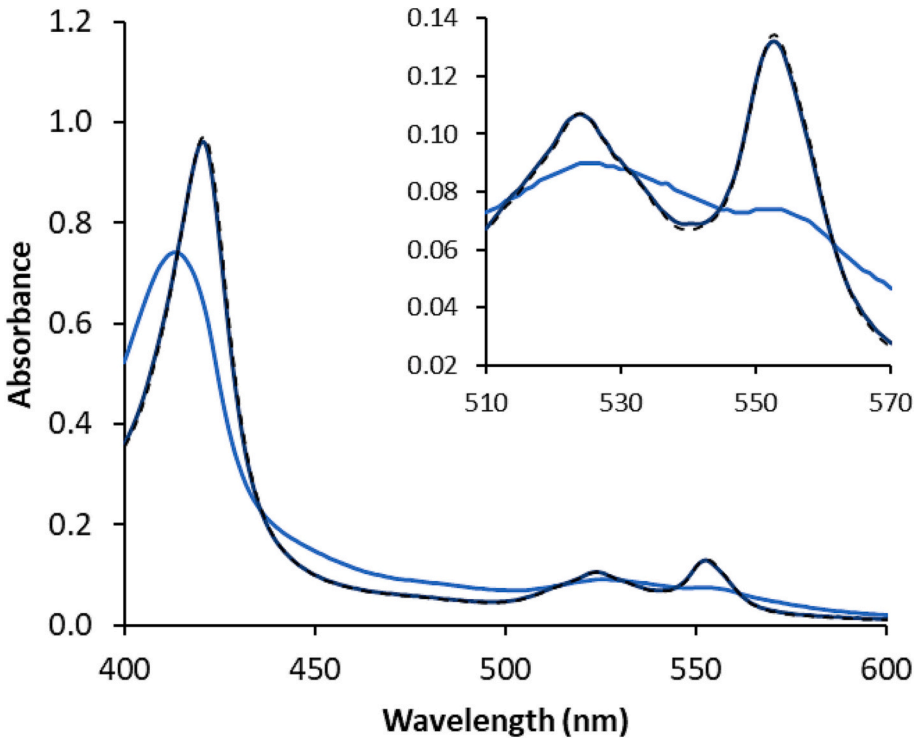

Fig. 8. Reduction of ACIII with menaquinol-4. UV–visible absorbance spectra of 20 μM of oxidized ACIII (light blue line), under anaerobic conditions, and reduced in the presence of menaquinol-4 (dark blue line) and dithionite (dashed black line). The inserted figure expands absorption spectrum in the 510–570 nm region. (For interpretation of the references to colour in this figure legend, the reader is referred to the web version of this article.)

quinone derivative identified as an inhibitor of quinone/quinol interacting enzymes, namely of the bc_1 complex [34], lowered the activity of the complex by 25 % (data not shown). The menaquinol:cytochrome *c* oxidoreductase activity showed maximal activity at 65 °C, consistent with the optimum temperature of growth of *R. marinus* [2].

3.2. Electrogenicity of ACIII

When ACIII was incorporated in liposomes containing menaquinone-4, prepared with *E. coli* phospholipids, the activity was 36.3 ± 3.2 s^{-1} (120.8 ± 10.6 nmol.mg^{-1}.s^{-1}) (Fig. 3, proteoliposomes). To investigate whether menaquinol:cytochrome *c* oxidoreductase activity is electrogenic, *i.e.*, coupled to the generation of a transmembrane electrochemical gradient, as previously proposed [10], we tested the effect of ionophores. The menaquinol:cytochrome *c* oxidoreductase activity increased in the presence of valinomycin (44.2 ± 3.1 s^{-1}, 147.2 ± 10.2 nmol.mg^{-1}.s^{-1}) or protonophore CCCP (45.4 ± 1.2 s^{-1}, 151.2 ± 3.8 nmol.mg^{-1}.s^{-1}) (Fig. 3).

3.3. Quinone binding-site

ACIII has one quinone-binding site on the periplasmic-side of the membrane, within suitable distance for electron-transfer to the redox centers [10]. A tryptophan fluorescence quenching assay of ACIII was performed in the presence of increasing amounts of menaquinone-4 (Fig. 4). Dissociation constant (K_d) of 23.9 ± 2.1 μM was obtained, considering a single binding site (Eq. 1).

3.4. Electron transfer between ACIII and its electron acceptors

To further understand the interactions between ACIII and its potential electron acceptors, we investigated the electron transfer from ACIII to the high potential iron-sulfur protein (HiPIP), the soluble cytochrome *c* (cytC) and the cytochrome *c* domain of the subunit II from the caa_3 reductase (domC). Previous work has established that ACIII is able to transfer electrons to the HiPIP [11], cytC [3] and to caa_3 oxygen reductase [9]. A comparison of the obtained turnover values, for menaquinol:electron acceptor oxidoreductase activity of ACIII (Fig. 5), revealed that the reduction of domC (18.5 ± 1.4 s^{-1}, 69.7 ± 5.1 nmol.mg^{-1}.s^{-1}) was significantly faster than the reduction of HiPIP or cytC, 4 ± 0.7 s^{-1} (15.1 ± 2.6 nmol.mg^{-1}.s^{-1}) and 7.6 ± 1.1 s^{-1} (28.6 ± 4.1 nmol.mg^{-1}.s^{-1}), respectively.

3.5. Binding affinities between ACIII and its electron acceptors

^{1}H-1D-NMR spectroscopy have been shown to be a suitable method to detect transient interactions between redox proteins in the oxidized state, through observation of changes in the chemical shifts (δ) of heme methyl resonances [31,35–39]. Consequently, the interaction between ACIII and its electron acceptors was evaluated by ^{1}H-^{1}D-NMR, using ActE, the monoheme subunit of ACIII instead of the whole complex, because it is the last electron acceptor within ACIII and mediates the electron transfer between ACIII and the caa_3 oxygen reductase [9,15]. The chemical shift perturbations for the heme methyl resonances of ActE were monitored upon the addition of increasing amounts of HiPIP (Fig. 6), cytC or domC.

From the evaluation of the chemical shift perturbations of ActE/electron acceptor we calculated dissociation constants (K_d) of 2.13 mM, 1.23 mM, and 0.79 mM for HiPIP, cytC and domC, respectively (Fig. 7). These values are within the range, consistent with other K_d values reported for the interaction between electron transfer proteins [36,37,40,41].

3.6. Electron transfer pathways

The prosthetic groups of ACIII form two electron transfer wires that diverge at the $[3Fe\text{-}4S]^{1+/0}$ cluster [10], one constituted by the heme groups of ActA and ActE and the other by the iron-sulfur cluster present

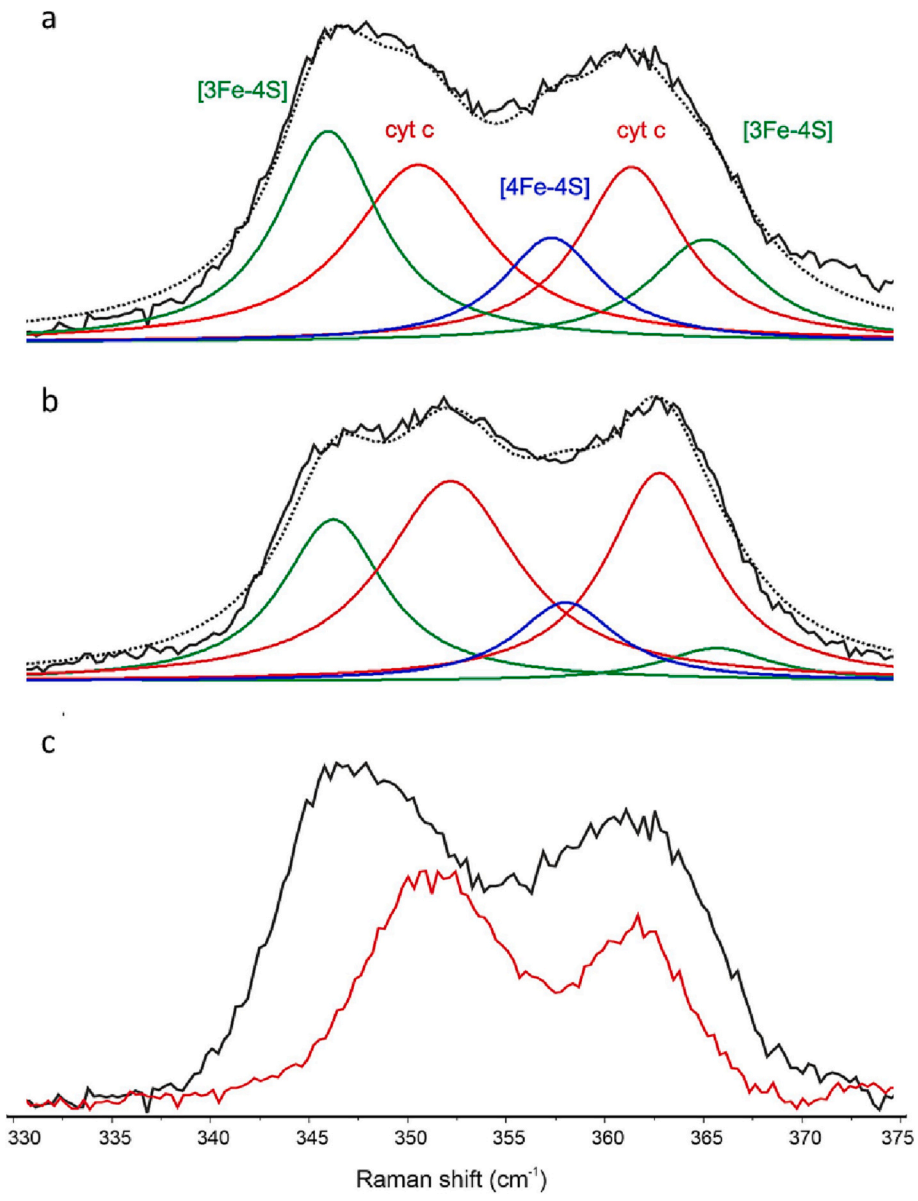

Fig. 9. Resonance Raman spectra of ACIII. a-b Experimental Resonance Raman spectra of ACIII (black) and spectra deconvoluted by component analysis (overall - black dotted line, individual components - colour coded) in oxidized (a) and menaquinol-4 reduced (b) states (green traces, $[3Fe\text{-}4S]^{1+}$, blue trace $[4Fe\text{-}4S]^{2+}$ cluster bands, red traces, heme bands). c Resonance Raman spectrum of ACIII in oxidized state (black) and oxidized soluble truncated monoheme cytochrome *c* subunit of ACIII (ActE, red). (For interpretation of the references to colour in this figure legend, the reader is referred to the web version of this article.)

in ActB. Full reduction of the hemes upon quinol oxidation was here observed (Fig. 8), supporting the role of the heme wire in the electron transfer.

Due to the proximity of the fourth $[4Fe\text{-}4S]^{2+/1+}$ cluster to the surface of ActB (~ 7 Å), it is reasonable to assume that the $[4Fe\text{-}4S]^{2+/1+}$ clusters wire might also have a role in electron transfer, however the characterization of these clusters has not been possible up to date [3].

We could never observe the $[4Fe\text{-}4S]^{2+/1+}$ clusters by EPR even in the presence of dithionite and changing temperature and power saturation conditions. The obtained RR data show the presence of $[4Fe\text{-}4S]^{2+/1+}$ clusters and suggest that these maybe redox active in the presence of menaquinol. Component analysis of the RR spectrum of ACIII in oxidized state (Fig. 9a) reveals a number of bands in the low frequency (340–375 cm^{-1}) region that can be attributed to heme and FeS moieties [42,43]. In particular, the bands at 346 and 366 cm^{-1} are indicative of $[3Fe\text{-}4S]^{1+}$ and that at 358 cm^{-1} of $[4Fe\text{-}4S]^{2+}$ clusters; the relative band intensities suggest a higher abundance of the latter [32]. Upon reduction of the protein with menaquinol-4 (Fig. 9b), the intensity of RR bands of (both types of) FeS clusters decrease (in comparison with those originating from heme groups). This indicates a partial reduction of the clusters to RR silent $[4Fe\text{-}4S]^{1+}$ and $[3Fe\text{-}4S]^{0}$ states and therefore their redox activity.

4. Discussion

ACIII, with a central role in the respiratory chain of *R. marinus*, is a menaquinol:cytochrome *c*/HiPIP oxidoreductase. The results presented here show that the membrane environment is crucial for the catalytic activity of ACIII. In particular, cardiolipin was essential to restore the menaquinol:cytochrome *c* oxidoreductase activity of a nearly inactive detergent-solubilized ACIII. Interestingly, it is one of the phospholipids identified in highest amount in *R. marinus* membranes [44,45]. The structure of ACIII from *R. marinus* and *Flavobacterium johnsoniae* revealed phospholipid molecules in the cytoplasmic interface between the membrane subunits ActC and ActF and near the proposed entry point for menaquinol into the complex [10,46]. Furthermore, other bacterial respiratory complexes, such as nitrate reductase (NarGHI) [47] and formate dehydrogenase-N (Fdn-N) [48], members of the CISM superfamily, to which ACIII is related to [13], were reported as being structurally and functionally dependent on cardiolipin.

One quinol-binding site located at the periplasmic side of the membrane was identified in ACIII. The quinol pocket in ActC is in a region of

the protein that is buried in the membrane, at approximately 10 Å from the $[3Fe\text{-}4S]^{1+/0}$ in ActB, implying this iron-sulfur cluster as the primary electron acceptor from the menaquinol [10]. All prosthetic groups of ACIII are located in the periplasm and form two electron transfer wires that diverge at the $[3Fe\text{-}4S]^{1+/0}$. Menaquinol was observed to reduce the hemes from both ActA and ActE and consequently to reduce the caa_3 oxygen reductase [15], showing the role of the heme wire in the electron transfer. The iron-sulfur clusters of ACIII were partially reduced in the presence of menaquinol-4. The cysteine motifs, involved in iron-sulfur cluster binding, are conserved in all ACIIIs sequences [13]. The retention of these sites may be indicative of a relevant role of the iron-sulfur pathway. Also, the third $[4Fe\text{-}4S]^{2+/1+}$ cluster (from the $[3Fe\text{-}4S]^{1+/0}$ center) is only located at ~7 Å beneath the protein surface [10] and it could be involved in a redox reaction with a unknown soluble protein. Nonetheless, there are examples of iron-sulfur clusters that seem not to participate in electron transfer, such as the case of Complex I, in which the iron-sulfur clusters N1a and N7 are conserved but do not participate in the electron transfer between NADH and the quinone [49].

We observed that ACIII interacts directly with caa_3 oxygen reductase, as well as with two electron carriers, the HiPIP and the soluble cytochrome *c*. ACIII is able to couple the oxidation of menaquinol to the reduction of HiPIP [11], cytC [3] and caa_3 oxygen reductase [9]. The data obtained in the present work show that ACIII interacted with HiPIP, cytC and domain *c* from subunit II of the caa_3 oxygen reductase. The dissociation constant (K_d) values, in the mM range, indicate the formation of low-affinity complexes between ACIII and the tested electron acceptors, which are consistent with transient interaction expected for inter proteins electron transfer. The affinity between the subunit ActE and the cytochrome *c* domain of subunit II of caa_3 oxygen reductase (domC) (K_d = 789 μM) presents the faster measured turnover (18.5 ± 1.4 s^{-1}, 69.7 ± 5.1 $nmol.mg^{-1}.s^{-1}$), supporting the idea that direct interaction between ACIII and caa_3 oxygen reductase is the preferred mode for electron transfer [9,10,15]. Moreover, the structure of ACIII from *R. marinus* provided evidence for the existence of a supercomplex between ACIII and the caa_3 oxygen reductase [10,15], but a physiological interaction between ACIII and HiPIP or cytochrome *c* cannot be ruled out.

ACIII has only one quinol-binding site and no cofactors in the membrane subunits [10], contrary to the cytochrome bc_1 complex, which led to the hypothesis that ACIII operates by a redox-driven proton translocation mechanism [10]. In fact, two putative proton pathways were described in the membrane subunits of ACIII [10]. The activity of ACIII reconstituted in liposomes increased in the presence of valinomycin and CCCP, two ionophores that disrupt the transmembrane electrochemical potential. Although statistically relevant, the activity in the presence of CCCP did not increase as much as observed for most respiratory enzymes [50,51]. It might be related to the possibility that at 65 °C proteoliposomes might not be so tight. Nevertheless, these are still capable of sustaining a membrane potential as activity increases in the presence of CCCP. These observations indicated that ACIII may be electrogenic. The QrcABCD complex, a Type I cytochrome c_3:menaquinone oxidoreductase related to the ACIII complex, was shown to be electrogenic [52].

The electron flow within ACIII is still unknown, however the presence of two functional electron transfer pathways cannot be ruled out, since upon menaquinol oxidation the hemes and the iron-sulfur clusters are reduced. With two functional electron transfer pathways, one electron of the menaquinol could be transferred to the iron-sulfur clusters of ActB and then to an electron acceptor. The other electron from menaquinol would flow to the hemes of ActA and ActE and then to the caa_3 oxygen reductase or a soluble electron carrier, such as HiPIP or the soluble cytochrome *c*.

The versatility of ACIII to have different electron acceptors, caa_3 oxygen reductase, HiPIP and the soluble cytochrome *c*, suggests the use of alternative electron pathways determined, for example by different metabolic conditions [53]. In this way, our results highlight the remarkable diversity and flexibility of Bacteria, with multiple electron pathways to terminal respiratory oxidases [20].

Declaration of competing interest

The authors declare that they have no known competing financial interests or personal relationships that could have appeared to influence the work reported in this paper.

Data availability

Data will be made available on request.

Acknowledgments

The work was funded by Fundação para a Ciência e a Tecnologia (PTDC/BIA-BQM/30528/2017). The project was further supported by UIDB/04046/2020 and UIDP/04046/2020 Centre grants from FCT, Portugal (to BioISI), by LISBOA-01-0145-FEDER-007660 cofunded by FEDER through COMPETE2020-POCI and by Fundação para a Ciência e a Tecnologia and by UIDB/04612/2020 and UIDP/04612/2020 research unit grants from FCT (to Mostmicro). This work benefited from access to CERMAX, ITQB-NOVA, Oeiras, Portugal with equipment funded by FCT, project AAC 01/SAICT/2016.

pMSP1D1 was a gift from Stephen Sligar (Addgene plasmid # 20061; http://n2t.net/addgene:20061; RRID:Addgene_20061).

References

[1] G.A. Alfredsson, J.K. Kristjansson, S. Hjorleifsdottir, K.O. Stetter, Rhodothermus marinus, gen. nov., sp. nov., a thermophibic, halophilic bacterium from submarine hot springs in Iceland, J. Gen. Microbiol. 134 (1988) 299–306, https://doi.org/10.1099/00221287-134-2-299.

[2] O.C. Nunes, M.M. Donato, M.S.Da Costa, Isolation and Characterization of Rhodothermus Strains from S. Miguel, Azores, Syst. Appl. Microbiol. 15 (1992) 92–97, https://doi.org/10.1016/S0723-2020(11)80144-X.

[3] M.M. Pereira, J.N. Carita, M. Teixeira, Membrane-bound electron transfer chain of the thermohalophilic bacterium Rhodothermus marinus: a novel multihemic cytochrome bc, a new complex III, Biochemistry 38 (1999) 1268–1275, https://doi.org/10.1021/bi9818063.

[4] M.M. Pereira, M. Santana, C.M. Soares, J. Mendes, J.N. Carita, A.S. Fernandes, M. Saraste, M.A. Carrondo, M. Teixeira, M. Soares, J. Mendes, M. Teixeira, M. M. Pereira, M. Santana, C.M. Soares, J. Mendes, J.N. Carita, A.S. Fernandes, M. Saraste, M.A. Carrondo, M. Teixeira, The caa3 terminal oxidase of the thermohalophilic bacterium Rhodothermus marinus: a HiPIP:oxygen oxidoreductase lacking the key glutamate of the D-channel, Biochim. Biophys. ActaBioenerg. 1413 (1999) 1–13, https://doi.org/10.1016/S0005-2728(99)00073-0.

[5] A.S. Fernandes, M.M. Pereira, M. Teixeira, The succinate dehydrogenase from the thermohalophilic bacterium Rhodothermus marinus: redox-Bohr effect on heme bL1, J. Bioenerg. Biomembr. 33 (2001) 343–352, https://doi.org/10.1023/A:1010663424846.

[6] A.S. Fernandes, M.M. Pereira, M. Teixeira, Purification and characterization of the complex I from the respiratory chain of Rhodothermus marinus, J. Bioenerg. Biomembr. 34 (2002) 413–421, https://doi.org/10.1023/A:1022509907553.

[7] A.F. Veríssimo, M.M. Pereira, A.M.P.P. Melo, G.O. Hreggvidsson, J.K. Kristjansson, M. Teixeira, A ba3 oxygen reductase from the thermohalophilic bacterium Rhodothermus marinus, FEMS Microbiol. Lett. 269 (2007) 41–47, https://doi.org/10.1111/j.1574-6968.2006.00598.x.

[8] P.N. Refojo, M.A. Ribeiro, F. Calisto, M. Teixeira, M.M. Pereira, Structural composition of alternative complex III: variations on the same theme, Biochim. Biophys. ActaBioenerg. 2013 (1827) 1378–1382, https://doi.org/10.1016/j.bbabio.2013.01.001.

[9] P.N. Refojo, F. Calisto, M.A. Ribeiro, M. Teixeira, M.M. Pereira, The monoheme cytochrome c subunit of Alternative Complex III is a direct electron donor to caa3 oxygen reductase in Rhodothermus marinus, Biol. Chem. 398 (2017) 1037–1044, https://doi.org/10.1515/hsz-2016-0323.

[10] J.S. Sousa, F. Calisto, J.D. Langer, D.J. Mills, P.N. Refojo, M. Teixeira, W. Kühlbrandt, J. Vonck, M.M. Pereira, Structural basis for energy transduction by respiratory alternative complex III, Nat. Commun. 9 (2018) 1728, https://doi.org/10.1038/s41467-018-04141-8.

[11] M.M. Pereira, J.N. Carita, M. Teixeira, Membrane-bound electron transfer chain of the thermohalophilic bacterium Rhodothermus marinus: characterization of the iron-sulfur centers from the dehydrogenases and investigation of the high-potential iron-sulfur protein function by in vitro reconstitu, Biochemistry 38 (1999) 1276–1283, https://doi.org/10.1021/bi981807v.

[12] M.M. Pereira, P.N. Refojo, G.O. Hreggvidsson, S. Hjorleifsdottir, M. Teixeira, The alternative complex III from Rhodothermus marinus - a prototype of a new family of quinol:electron acceptor oxidoreductases, FEBS Lett. 581 (2007) 4831–4835, https://doi.org/10.1016/j.febslet.2007.09.008.
[13] P.N. Refojo, F.L. Sousa, M. Teixeira, M.M. Pereira, The alternative complex III: a different architecture using known building modules, Biochim. Biophys. ActaBioenerg. 1797 (2010) 1869–1876, https://doi.org/10.1016/j.bbabio.2010.04.012.
[14] M.M. Pereira, F. Calisto, P.N. Refojo, Bioenergetics theory and components | respiratory alternative complex III – structural and functional insights, in: Encycl. Biol. Chem. III, Elsevier, 2021, pp. 143–149, https://doi.org/10.1016/B978-0-12-809633-8.21535-5.
[15] P.N. Refojo, M. Teixeira, M.M. Pereira, The alternative complex III ofRhodothermus marinus and its structural and functional association with caa3 oxygen reductase, Biochim. Biophys. ActaBioenerg. 1797 (2010) 1477–1482, https://doi.org/10.1016/j.bbabio.2010.02.029.
[16] F. Calisto, M.M. Pereira, The ion-translocating NrfD-like subunit of energy-transducing membrane complexes, Front. Chem. 9 (2021), https://doi.org/10.3389/fchem.2021.663706.
[17] F. Calisto, M.M. Pereira, Modularity of membrane-bound charge-translocating protein complexes, Biochem. Soc. Trans. 49 (2021) 2669–2685, https://doi.org/10.1042/BST20210462.
[18] P.N. Refojo, M. Teixeira, M.M. Pereira, The alternative complex III: properties and possible mechanisms for electron transfer and energy conservation, Biochim. Biophys. ActaBioenerg. 2012 (1817) 1852–1859, https://doi.org/10.1016/j.bbabio.2012.05.003.
[19] F. Calisto, F.M. Sousa, F.V. Sena, P.N. Refojo, M.M. Pereira, Mechanisms of energy transduction by charge translocating membrane proteins, Chem. Rev. 121 (2021) 1804–1844, https://doi.org/10.1021/acs.chemrev.0c00830.
[20] B.C. Marreiros, F. Calisto, P.J. Castro, A.M. Duarte, F.V. Sena, A.F. Silva, F. M. Sousa, M. Teixeira, P.N. Refojo, M.M. Pereira, Exploring membrane respiratory chains, Biochim. Biophys. ActaBioenerg. 2016 (1857) 1039–1067, https://doi.org/10.1016/j.bbabio.2016.03.028.
[21] M.M. Pereira, J.N. Carita, R. Anglin, M. Saraste, M. Teixeira, Heme centers of Rhodothermus marinus respiratory chain. Characterization of its cbb3 oxidase, J. Bioenerg. Biomembr. 32 (2000) 143–152, https://doi.org/10.1023/A:1005555829301.
[22] V. Srinivasan, C. Rajendran, F.L. Sousa, A.M.P.P. Melo, L.M. Saraiva, M.M. Pereira, M. Santana, M. Teixeira, H. Michel, Structure at 1.3 Å resolution of Rhodothermus marinus caa3cytochrome c domain, J. Mol. Biol. 345 (2005) 1047–1057, https://doi.org/10.1016/j.jmb.2004.10.069.
[23] M. Stelter, A.M.P.P. Melo, M.M. Pereira, C.M. Gomes, G.O. Hreggvidsson, S. Hjorleifsdottir, L.M. Saraiva, M. Teixeira, M. Archer, A novel type of monoheme cytochrome c: biochemical and structural characterization at 1.23 Å resolution of Rhodothermus marinus cytochrome c, Biochemistry 47 (2008) 11953–11963, https://doi.org/10.1021/bi800999g.
[24] M. Stelter, A.M.P.P. Melo, G.O. Hreggvidsson, S. Hjorleifsdottir, L.M. Saraiva, M. Teixeira, M. Archer, Structure at 1.0 Å resolution of a high-potential iron-sulfur protein involved in the aerobic respiratory chain of Rhodothermus marinus, J. Biol. Inorg. Chem. 15 (2010) 303–313, https://doi.org/10.1007/s00775-009-0603-8.
[25] T.K. Ritchie, Y.V. Grinkova, T.H. Bayburt, I.G. Denisov, J.K. Zolnerciks, W. M. Atkins, S.G. Sligar, Reconstitution of membrane proteins in phospholipid bilayer nanodiscs, Methods Enzymol. (2009) 211–231, https://doi.org/10.1016/S0076-6879(09)64011-8.
[26] I.G. Denisov, Y.V. Grinkova, A.A. Lazarides, S.G. Sligar, Directed self-assembly of monodisperse phospholipid bilayer nanodiscs with controlled size, J. Am. Chem. Soc. 126 (2004) 3477–3487, https://doi.org/10.1021/ja0393574.
[27] C.L. Ragan, M.T. Wilson, V.M. Darley-Usmar, P.N. Lowe, Subfractionation of mitochondria and isolation of the proteins of oxidative phosphorylation, in: Mitochondria A Prat. Approach, IRL Press, Oxford, 1987, pp. 79–122.
[28] E. Margoliash, N. Frohwirt, Spectrum of horse-heart cytochrome c, Biochem. J. 71 (1959) 570–572, https://doi.org/10.1042/bj0710570.
[29] S.M. Akbar, K. Sreeramulu, H.C. Sharma, Tryptophan fluorescence quenching as a binding assay to monitor protein conformation changes in the membrane of intact mitochondria, J. Bioenerg. Biomembr. 48 (2016) 241–247, https://doi.org/10.1007/s10863-016-9653-0.
[30] I. Díaz-Moreno, A. Díaz-Quintana, M. Ubbink, M.A. De la Rosa, An NMR-based docking model for the physiological transient complex between cytochrome f and cytochrome c 6, FEBS Lett. 579 (2005) 2891–2896, https://doi.org/10.1016/j.febslet.2005.04.031.
[31] J.A.R. Worrall, W. Reinle, R. Bernhardt, M. Ubbink, Transient protein interactions studied by NMR spectroscopy: the case of cytochrome c and adrenodoxin, Biochemistry 42 (2003) 7068–7076, https://doi.org/10.1021/bi0342968.
[32] S. Todorovic, S.S. Leal, C.A. Salgueiro, I. Zebger, P. Hildebrandt, D.H. Murgida, C. M. Gomes, A spectroscopic study of the temperature induced modifications on ferredoxin folding and iron−sulfur moieties, Biochemistry 46 (2007) 10733–10738, https://doi.org/10.1021/bi700967g.
[33] X. Gao, Y. Xin, R.E. Blankenship, Enzymatic activity of the alternative complex III as a menaquinol:auracyanin oxidoreductase in the electron transfer chain of Chloroflexus aurantiacus, FEBS Lett. 583 (2009) 3275–3279, https://doi.org/10.1016/j.febslet.2009.09.022.
[34] M.D. Esposti, A.-L. Tsai, G. Palmer, G. Lenaz, On the oxidation pathways of the mitochondrial bc1 complex from beef heart. Effects of various inhibitors, Eur. J. Biochem. 160 (1986) 547–555, https://doi.org/10.1111/j.1432-1033.1986.tb10073.x.
[35] I.B. Coutinho, D.L. Turner, J. Legall, A.V. Xavier, NMR studies and redox titration of the tetraheme cytochrome c 3 from Desulfomicrobium baculatum. Identification of the low-potential heme, Eur. J. Biochem. 230 (1995) 1007–1013, https://doi.org/10.1111/j.1432-1033.1995.tb20649.x.
[36] B.M. Fonseca, C.M. Paquete, S.E. Neto, I. Pacheco, C.M. Soares, R.O. Louro, Mind the gap: cytochrome interactions reveal electron pathways across the periplasm of Shewanella oneidensis MR-1, Biochem. J. 449 (2013) 101–108, https://doi.org/10.1042/BJ20121467.
[37] M.N. Alves, S.E. Neto, A.S. Alves, B.M. Fonseca, A. Carrêlo, I. Pacheco, C. M. Paquete, C.M. Soares, R.O. Louro, Characterization of the periplasmic redox network that sustains the versatile anaerobic metabolism of Shewanella oneidensis MR-1, Front. Microbiol. 6 (2015) 665, https://doi.org/10.3389/fmicb.2015.00665.
[38] E.R.P. Zuiderweg, Mapping protein−protein interactions in solution by NMR spectroscopy †, Biochemistry 41 (2002) 1–7, https://doi.org/10.1021/bi011870b.
[39] J.L. Ortega-Roldan, M. Blackledge, M.R. Jensen, Characterizing protein-protein interactions using solution NMR Spectroscopy, in: Protein Complex Assem, 2018, pp. 73–85, https://doi.org/10.1007/978-1-4939-7759-8_5.
[40] J.R. Perkins, I. Diboun, B.H. Dessailly, J.G. Lees, C. Orengo, Transient protein-protein interactions: structural, functional, and network properties, Structure 18 (2010) 1233–1243, https://doi.org/10.1016/j.str.2010.08.007.
[41] C.M. Paquete, B.M. Fonseca, D.R. Cruz, T.M. Pereira, I. Pacheco, C.M. Soares, R. O. Louro, Exploring the molecular mechanisms of electron shuttling across the microbe/metal space, Front. Microbiol. 5 (2014) 318, https://doi.org/10.3389/fmicb.2014.00318.
[42] S. Todorovic, M. Teixeira, Resonance Raman spectroscopy of Fe–S proteins and their redox properties, J. Biol. Inorg. Chem. 23 (2018) 647–661, https://doi.org/10.1007/s00775-018-1533-0.
[43] G. Caserta, L. Zuccarello, C. Barbosa, C.M. Silveira, E. Moe, S. Katz, P. Hildebrandt, I. Zebger, S. Todorovic, Unusual structures and unknown roles of FeS clusters in metalloenzymes seen from a resonance Raman spectroscopic perspective, Coord. Chem. Rev. 452 (2022), 214287, https://doi.org/10.1016/j.ccr.2021.214287.
[44] B.J. Tindall, Lipid composition of Rhodothermus marinus, FEMS Microbiol. Lett. 80 (1991) 65–68, https://doi.org/10.1111/j.1574-6968.1991.tb04637.x.
[45] O.C. Nunes, M.M. Donato, C.M. Manaia, M.S. Da Costa, The polar lipid and fatty acid composition of Rhodothermus strains, Syst. Appl. Microbiol. 15 (1992) 59–62, https://doi.org/10.1016/S0723-2020(11)80139-6.
[46] C. Sun, S. Benlekbir, P. Venkatakrishnan, Y. Wang, S. Hong, J. Hosler, E. Tajkhorshid, J.L. Rubinstein, R.B. Gennis, Structure of the alternative complex III in a supercomplex with cytochrome oxidase, Nature 557 (2018) 123–126, https://doi.org/10.1038/s41586-018-0061-y.
[47] R. Arias-Cartin, S. Grimaldi, J. Pommier, P. Lanciano, C. Schaefer, P. Arnoux, G. Giordano, B. Guigliarelli, A. Magalon, Cardiolipin-based respiratory complex activation in bacteria, Proc. Natl. Acad. Sci. U. S. A. 108 (2011) 7781–7786, https://doi.org/10.1073/pnas.1010427108.
[48] M. Jormakka, S. Törnroth, B. Byrne, S. Iwata, Molecular basis of proton motive force generation: structure of formate dehydrogenase-N, Science (80-.) 295 (2002) 1863–1868, https://doi.org/10.1126/science.1068186.
[49] P. Hinchliffe, L.A. Sazanov, Organization of iron-sulfur clusters in respiratory complex I, Science(80-.) 309 (2005) 771–774, https://doi.org/10.1126/science.1113988.
[50] A. Galkin, S. Dröse, U. Brandt, The proton pumping stoichiometry of purified mitochondrial complex I reconstituted into proteoliposomes, Biochim. Biophys. ActaBioenerg. 1757 (2006) 1575–1581, https://doi.org/10.1016/j.bbabio.2006.10.001.
[51] H. Rottenberg, R. Covian, B.L. Trumpower, Membrane potential greatly enhances superoxide generation by the cytochrome bc1 complex reconstituted into phospholipid vesicles, J. Biol. Chem. 284 (2009) 19203–19210, https://doi.org/10.1074/jbc.M109.017376.
[52] A.G. Duarte, T. Catarino, G.F. White, D. Lousa, S. Neukirchen, C.M. Soares, F. L. Sousa, T.A. Clarke, I.A.C. Pereira, An electrogenic redox loop in sulfate reduction reveals a likely widespread mechanism of energy conservation, Nat. Commun. 9 (2018) 5448, https://doi.org/10.1038/s41467-018-07839-x.
[53] F. Alberge, L. Espinosa, F. Seduk, L. Sylvi, R. Toci, A. Walburger, A. Magalon, Dynamic subcellular localization of a respiratory complex controls bacterial respiration, elife 4 (2015), e05357, https://doi.org/10.7554/eLife.05357.